Dynamical and phase-diagram study on stable optical pulling force in Bessel beams

Neng Wang,[1,2] Jun Chen,[1,3,*] Shiyang Liu,[1,4,†] and Zhifang Lin[1,2]

[1]*State Key Laboratory of Surface Physics (SKLSP) and Department of Physics, Fudan University, Shanghai 200433, China*

[2]*Key Laboratory of Micro and Nano Photonic Structures (Ministry of Education), Fudan University, Shanghai 200433, China*

[3]*Institute of Theoretical Physics and Department of Physics, Shanxi University, Taiyuan 030006, China*

[4]*Institute of Information Optics, Zhejiang Normal University, Jinhua, Zhejiang 321004, China*

(Received 3 March 2013; published 10 June 2013)

Based on the generalized Lorenz-Mie theory and Maxwell stress tensor formulism, we calculate the transverse force constant matrix and perform a linear stability analysis on a spherical particle that is subject to negative longitudinal optical force (NLOF) under the illumination of Bessel beams. Phase diagrams with respect to the material parameters are presented, which exhibit the possibility of the appearance of NLOF. From dynamical simulations of the particle performed both in the transverse plane and along the longitudinal direction, an even clearer picture of the realization of stable NLOF is presented. It is shown that, due to rotation induced by the orbital angular-momentum of light, higher order Bessel beams cannot stably confine a particle to the beam center where NLOF occurs in the absence of ambient damping, which largely limits their applications for long-distance, stable, backward particle transportation. On the other hand, zero-order Bessel beams can achieve stable transverse confinement of the manipulated particle and act as an optical tractor beam *per se*. In addition, for a nonmagnetic particle with relative permeability $\mu = 1$, a Bessel beam with transverse electric polarization is more favorable for the realization of NLOF than a transverse magnetic beam. Finally, a brief discussion is also presented of the conditions under which an off-beam-axis particle could be suitable for backward transportation using NLOF.

DOI: 10.1103/PhysRevA.87.063812 PACS number(s): 42.50.Wk, 87.80.Cc, 78.70.−g, 42.15.Dp

I. INTRODUCTION

There has been a surge of interest in negative optical force [1–11] and negative acoustical force [12–15], where a particle located in an optical or acoustical beam is subject to a radiation force opposite to the direction of beam propagation. The negative forces originate physically from the simultaneous excitation of multipoles in the particle and the strong forward scattering produced by the interference of these multipoles [4]. They provide for optical or acoustical manipulation [16–24] with a novel third handle, optical (acoustical) pulling, in addition to the conventional well-known optical trapping and binding. However, nearly all attention has been focused on the demonstration of negative optical force by searching in beam and particle parameters, such as the numerical aperture and polarization of operating beam, as well as the permeability, permittivity, and size of particle, little has been done to study the transverse trapping stability of the particle in regions where negative longitudinal optical force (NLOF) occurs. Actually, if the particle cannot be confined transversely within the region where it is subject to NLOF, all the results of NLOF become meaningless and irrelevant. For instance, regarding a beam carrying orbital angular momentum (OAM) [25,26], while the linear momentum of light exerts optical force on particles under its illumination, the OAM of light can also be delivered to particles, causing them to rotate, orbiting around the beam center [24,27,28], which is unfavorable for stable trapping. If the OAM-induced rotation dominates the restoring force due, mainly, to the field intensity gradient, then the particle may not be transversely confined near the point of the field extrema where NLOF occurs, especially in the absence of ambient damping. It may even escape from the transverse trap eventually, due to the accumulation of angular momentum (AM) acquired from the beam [28], ruining the practical scenarios of NLOF. As a result, the stability analysis on NLOF is of great importance for its practical applications.

In this paper, we present a transverse linear stability investigation of a spherical particle when it is subject to NLOF under the illumination of Bessel beams [29–35]. A detailed analysis is performed based on the phase diagrams with respect to material parameters and the force constant matrix (FCM) [28,36,37] as well as the dynamical simulations. The time-averaged optical force that acts on the particle is calculated via a surface integral of the time-averaged Maxwell stress tensor over the surface of the sphere. The electromagnetic fields involved in the Maxwell stress tensor are computed by the rigorous and accurate generalized Lorenz-Mie theory [38–40], where the field quantities are expanded in a series of vector spherical wave functions (VSWFs) [4,28,36,37,41–45]. The formulations can be considered *ab initio* within classical electrodynamics, in the sense that no approximation is required (up to numerical truncation). Our results show that if one uses Bessel beams [29–35] as the tractor beam, only a zero-order Bessel beam can achieve stable on-axis transverse trapping under both damping and undamping conditions. Although first-order Bessel beams may provide greater NLOF for a wider range of particle size and material parameters [4,6], due to OAM carried by beams the particle cannot be confined near the beam center without the help of ambient damping, which may largely limit practical applications. Finally, we also present a brief discussion on the conditions under which an off-beam-axis-located particle can be attracted to the beam center and pulled backward to the light source.

The rest of the paper is organized as follows. In Sec. II, we briefly describe the formulation for calculation of the optical force and the FCM based on the Lorenz-Mie theory and

*chenjun@sxu.edu.cn

†syliu@zjnu.cn

Maxwell stress tensor formalism. Analytical expressions for calculation of FCM as well as the optical force are presented. In Sec. III, we present the numerical results and discussion. Based on the phase diagrams and dynamical simulations, it is clearly demonstrated that due to the accompaniment of OAM, higher order Bessel beams cannot achieve stable NLOF in a dissipationless ambience, making them unfavorable for practical applications. Finally, conclusions are summarized in Sec. IV.

II. FORMULATIONS

In this section, we briefly recapitulate the generalized Lorenz-Mie theory and Maxwell tensor formulism for calculation of the optical force of a particle illuminated by Bessel beams. Emphasis is placed on the calculation of the FCM and its application to the linear stability analysis.

A. Calculation of optical force

A spherical particle of radius r placed in vacuum is considered, which has relative dielectric permittivity ε and relative magnetic permeability μ. It is illuminated by a Bessel beam of order l and propagating along the z axis of the beam coordinate system, with the electric field described by [30]

$$\boldsymbol{E}_i(\rho,\phi,z) = i c_1 \boldsymbol{M}_l^{(c)}(\rho,\phi,z) + c_2 \boldsymbol{N}_l^{(c)}(\rho,\phi,z), \tag{1}$$

where (ρ,ϕ,z) denote the cylindrical coordinates and time dependence $e^{-i\omega t}$ has been assumed and suppressed. The vector cylindrical wave functions (VCWFs) $\boldsymbol{M}_l^{(c)}(\rho,\phi,z)$ and $\boldsymbol{N}_l^{(c)}(\rho,\phi,z)$ are defined by [30]

$$\begin{aligned}\boldsymbol{M}_l^{(c)}(\rho,\phi,z) &= \left[\frac{il}{\rho} J_l(a\rho)\boldsymbol{e}_\rho - a J_l'(a\rho)\boldsymbol{e}_\phi\right] e^{il\phi+ibz},\\ \boldsymbol{N}_l^{(c)}(\rho,\phi,z) &= \frac{a^2}{k} J_l(a\rho)\boldsymbol{e}_z e^{il\phi+ibz} + \frac{ib}{k}\boldsymbol{e}_z \times \boldsymbol{M}_l^{(c)},\end{aligned} \tag{2}$$

with $J_l(x)$ and $J_l'(x)$ denoting, respectively, the Bessel function of order l and the derivative with respect to its argument. The coefficients c_1 and c_2 describe the complex amplitude of the transverse electric (TE; with the electric field polarized transverse to the propagation direction) and transverse magnetic (TM; with the magnetic field polarized transverse to the propagation direction) wave components, respectively. Superposition of the TE and TM modes provides a general propagation-invariant Bessel beam with complex polarizations [30,32,34]. When decomposed into plane-wave components, the Bessel beams given by Eq. (1) all have wave vectors of plane waves lying on a cone surface characterized by the cone angle α [30,32,34], with

$$a = k\sin\alpha \quad \text{and} \quad b = k\cos\alpha \tag{3}$$

denoting the transverse and longitudinal wave numbers, respectively, and $k = \omega/c$ being the wave number in vacuum.

Based on the generalized Lorenz-Mie theory, the incident electromagnetic field illuminating the spherical particle is expanded in terms of VSWFs centered at the particle, instead of at the origin of the beam coordinate system. So the electric field of the Bessel beam is cast into [46]

$$\boldsymbol{E}_i = -\sum_{n,m} i^{n+1}\gamma_{mn}\left[p_{mn}\boldsymbol{N}_{mn}^{(s1)} + q_{mn}\boldsymbol{M}_{mn}^{(s1)}\right], \tag{4}$$

where p_{mn} and q_{mn} are known as the partial wave expansion coefficients of the incident beam [36,41–45]. Throughout this paper, $\sum_{n,m}$ denotes the summation of n from 1 to ∞ and of m from $-n$ to n, and

$$\gamma_{mn} = \left[\frac{2n+1}{n(n+1)}\frac{(n-m)!}{(n+m)!}\right]^{1/2}. \tag{5}$$

The VSWFs $\boldsymbol{N}_{mn}^{(s1)}$ and $\boldsymbol{M}_{mn}^{(s1)}$ are based on spherical Bessel functions [36,41–44] and centered at the particle. For the incident Bessel beam, the partial wave expansion coefficients can be obtained by expanding VCWFs in terms of VSWFs. To study the case when the particle is located off the beam axis, VCWFs should be expanded in terms of VSWFs that have a different expansion center. The expansions have been worked out recently [45] based on the angular spectrum representation of an optical beam [47,48]. They are given by

$$\begin{aligned}\boldsymbol{M}_l^{(c)}(\rho,\phi,z) &= \sum_{n,m} i^{n+1}\gamma_{mn}\left[p_{mn}^{(b)}\boldsymbol{N}_{mn}^{(s1)} + q_{mn}^{(b)}\boldsymbol{M}_{mn}^{(s1)}\right],\\ \boldsymbol{N}_l^{(c)}(\rho,\phi,z) &= \sum_{n,m} i^{n+1}\gamma_{mn}\left[q_{mn}^{(b)}\boldsymbol{N}_{mn}^{(s1)} + p_{mn}^{(b)}\boldsymbol{M}_{mn}^{(s1)}\right],\end{aligned} \tag{6}$$

where [45]

$$\begin{aligned}p_{mn}^{(b)} &= i^{-m} J_{l-m}(a\rho_0)\, e^{i(l-m)\phi_0}\,\tilde{\pi}_{mn}(\cos\alpha)\, e^{ibz_0},\\ q_{mn}^{(b)} &= i^{-m} J_{l-m}(a\rho_0)\, e^{i(l-m)\phi_0}\,\tilde{\tau}_{mn}(\cos\alpha)\, e^{ibz_0},\end{aligned} \tag{7}$$

with (ρ_0,ϕ_0,z_0) denoting the cylindrical coordinates of the particle center in the beam coordinate system. The z_0 dependence appearing as e^{ibz_0} has no effect on the optical force and manifests the propagation-invariant property of Bessel beams [34]. In the following, the z_0 dependence is omitted for simplicity. Two auxiliary functions in Eq. (7) are related to the associated Legendre function of the first kind by

$$\begin{aligned}\tilde{\pi}_{mn}(\cos\alpha) &= \gamma_{mn}\frac{m P_n^m(\cos\alpha)}{\sin\alpha},\\ \tilde{\tau}_{mn}(\cos\alpha) &= \gamma_{mn}\frac{d P_n^m(\cos\alpha)}{d\alpha},\end{aligned} \tag{8}$$

with

$$\begin{aligned}P_n^m(x) &= \frac{1}{2^n n!}(1-x^2)^{m/2}\frac{d^{n+m}}{dx^{n+m}}[(x^2-1)^n],\\ P_n^{-m}(x) &= (-1)^m\frac{(n-m)!}{(n+m)!}P_n^m(x).\end{aligned} \tag{9}$$

It follows from Eqs. (1) and (6) that the partial wave expansion coefficients in Eq. (4) read

$$p_{mn} = -ic_1 p_{mn}^{(b)} - c_2 q_{mn}^{(b)}, \quad q_{mn} = -ic_1 q_{mn}^{(b)} - c_2 p_{mn}^{(b)}. \tag{10}$$

The scattered field from the particle is also expanded in terms of VSWFs centered at the particle

$$\boldsymbol{E}_s = \sum_{n,m} i^{n+1}\gamma_{mn}\left(a_{mn}\boldsymbol{N}_{mn}^{(s3)} + b_{mn}\boldsymbol{M}_{mn}^{(s3)}\right), \tag{11}$$

where $\boldsymbol{N}_{mn}^{(s3)}$ and $\boldsymbol{M}_{mn}^{(s3)}$ are VSWFs with their radial functions characterized by spherical Hankel functions of the first

kind [36,41–44] and centered at the particle. The scattering coefficients a_{mn} and b_{mn} are given by

$$a_{mn} = a_n p_{mn}, \quad b_{mn} = b_n q_{mn}, \tag{12}$$

with a_n and b_n denoting the Mie coefficients [42] of the particle.

With the partial wave expansion coefficients p_{mn} and q_{mn} as well as the scattering coefficients a_{mn} and b_{mn}, the time-averaged optical force $\boldsymbol{f} = f_x \boldsymbol{e}_x + f_y \boldsymbol{e}_y + f_z \boldsymbol{e}_z$ acting on the illuminated particle can be evaluated via a surface integral of the time-averaged Maxwell stress tensor over the surface of the particle [36,37,44,49–53]. When the background medium is lossless, the integration can be performed at infinity, due to conservation of momentum. This leads to much simplified expressions [36,43,44,54–58], which read, using the notations in the present paper,

$$f_x = \mathrm{Re}[F_1], \quad f_y = \mathrm{Im}[F_1], \quad f_z = \mathrm{Re}[F_2]. \tag{13}$$

The complex functions F_1 and F_2 are given by

$$\begin{aligned} F_1 &= \frac{2\pi\varepsilon_0}{k^2} \sum_{n,m} \left[c_{11} F_1^{(1)} + c_{12} F_1^{(2)} + c_{13} F_1^{(3)} \right], \\ F_2 &= -\frac{4\pi\varepsilon_0}{k^2} \sum_{n,m} \left[c_{21} F_2^{(1)} + c_{22} F_2^{(2)} \right], \end{aligned} \tag{14}$$

where ε_0 is the permittivity of the lossless background medium, and

$$\begin{aligned} F_1^{(1)} &= \tilde{a}_{mn} \tilde{b}^*_{m_1 n} + \tilde{b}_{mn} \tilde{a}^*_{m_1 n} - \tilde{p}_{mn} \tilde{q}^*_{m_1 n} - \tilde{q}_{mn} \tilde{p}^*_{m_1 n}, \\ F_1^{(2)} &= \tilde{a}_{mn} \tilde{a}^*_{m_1 n_1} + \tilde{b}_{mn} \tilde{b}^*_{m_1 n_1} - \tilde{p}_{mn} \tilde{p}^*_{m_1 n_1} - \tilde{q}_{mn} \tilde{q}^*_{m_1 n_1}, \\ F_1^{(3)} &= \tilde{a}_{mn_1} \tilde{a}^*_{m_1 n} + \tilde{b}_{mn_1} \tilde{b}^*_{m_1 n} - \tilde{p}_{mn_1} \tilde{p}^*_{m_1 n} - \tilde{q}_{mn_1} \tilde{q}^*_{m_1 n}, \\ F_2^{(1)} &= \tilde{a}_{mn} \tilde{a}^*_{mn_1} + \tilde{b}_{mn} \tilde{b}^*_{mn_1} - \tilde{p}_{mn} \tilde{p}^*_{mn_1} - \tilde{q}_{mn} \tilde{q}^*_{mn_1}, \\ F_2^{(2)} &= \tilde{a}_{mn} \tilde{b}^*_{mn} - \tilde{p}_{mn} \tilde{q}^*_{mn}, \end{aligned} \tag{15}$$

with $m_1 = m + 1$, $n_1 = n + 1$, a superscript asterisk denoting the complex conjugate, and

$$\begin{aligned} \tilde{a}_{mn} &= a_{mn} - \tfrac{1}{2} p_{mn}, \quad \tilde{p}_{mn} = \tfrac{1}{2} p_{mn}, \\ \tilde{b}_{mn} &= b_{mn} - \tfrac{1}{2} q_{mn}, \quad \tilde{q}_{mn} = \tfrac{1}{2} q_{mn}. \end{aligned} \tag{16}$$

The coefficients in Eq. (14) read

$$\begin{aligned} c_{11} &= \left[\frac{(n-m)(n+m+1)}{n^2(n+1)^2} \right]^{1/2}, \\ c_{12} &= -\left[\frac{n(n+2)(n+m+1)(n+m+2)}{(n+1)^2(2n+1)(2n+3)} \right]^{1/2}, \\ c_{13} &= \left[\frac{n(n+2)(n-m)(n-m+1)}{(n+1)^2(2n+1)(2n+3)} \right]^{1/2}, \\ c_{21} &= \left[\frac{n(n+2)(n-m+1)(n+m+1)}{(n+1)^2(2n+1)(2n+3)} \right]^{1/2}, \\ c_{22} &= \frac{m}{n(n+1)}. \end{aligned} \tag{17}$$

B. Linear stability analysis

When a particle is located on the beam axis of the incident Bessel beam, it is subject to a nonzero longitudinal optical force, either being pushed along the beam propagation path with $f_z > 0$ or being pulled backward to the light source with $f_z < 0$ [2–11]. In the transverse plane, the particle is in equilibrium due to the transverse field gradient. But this transverse equilibrium can be stable, unstable, or quasistable [28,36]. To realize any practical scenario for the application of NLOF, stable transverse trapping must be fulfilled. In the following, we summarize the basic formulism of a linear stability analysis which is efficient in judging the stability of a trapped particle.

Assume that a particle illuminated by a general optical beam propagating along z is placed at its transverse equilibrium with $f_x = f_y = 0$. When the particle deviates slightly from the transverse equilibrium, the transverse optical force $\boldsymbol{f}_t$ and ambient damping force $\boldsymbol{f}_d$ appear, which satisfies $\boldsymbol{f} = \boldsymbol{f}_t + \boldsymbol{f}_d = \widehat{\mathbf{K}} \Delta\boldsymbol{x} - \gamma d\Delta\boldsymbol{x}/dt$, with $\Delta\boldsymbol{x}$ the small displacement of the particle from the equilibrium and γ the ambient damping constant. Due to the symmetry, x and y can be decoupled from z. As a result, the submatrix $\widehat{\mathbf{K}}'$ is a 2×2 transverse FCM in the form

$$\widehat{\mathbf{K}}' = \begin{bmatrix} k_{11} & k_{12} \\ k_{21} & k_{22} \end{bmatrix}, \tag{18}$$

where all elements, given by $k_{ij} = \partial f_i / \partial(\Delta x_j)$, are real numbers. Here $f_i = f_x$ and f_y and $\Delta x_i = \Delta x$ and Δy for $i = 1$ and $=2$, respectively. When the diagonal elements, k_{11} and k_{22}, are both negative, they describe two restoring forces, usually taken as the two transverse stiffness constants in conventional approach. The off-diagonal element k_{12} (k_{21}) characterizes the optical force along the x (y) direction as the particle is displaced along y (x). These forces cause the particle to rotate around the beam axis [24,28,36]. For optical beams carrying OAM, the light energy moves forward spirally along the beam axis, giving rise to a rotating energy flux in the transverse plane. The rotating energy flux will deliver a torque on the particle, yielding the nonzero off-diagonal matrix components k_{12} and k_{21} [24,28,36]. As a result, the stability analysis for optical trapping should be started with the FCM, rather than the scheme based solely on the diagonal elements in the conventional approach [6].

The linear stability analysis is performed by diagonalizing the FCM in Eq. (18) to obtain two eigenvalues:

$$\lambda_\pm = \frac{(k_{11} + k_{22}) \pm \sqrt{(k_{11} - k_{22})^2 + 4k_{12}k_{21}}}{2}. \tag{19}$$

They give the eigen–force constants (EFCs; or *effective* transverse trap stiffnesses). In general, the eigenvalues can be complex. If either of the eigenvalues has a positive real part, then the transverse equilibrium is unstable. The stable equilibrium corresponds to two real and negative eigenvalues, where transverse trapping can be simply characterized by two stiffness constants along the principal axes that are determined by the eigenvectors of $\widehat{\mathbf{K}}'$. If, however, the eigenvalues turn out to be a conjugate pair of complex numbers with negative real part, then transverse trapping may not be naively characterized by two real force constants. The occurrence of complex EFCs

implies that the particle will orbit around the beam center with accelerating angular speed and, eventually, escape from the transverse trap in the absence of ambient dissipation, ruining the applicability of NLOF.

The linear stability analysis is made simple with the analytical expressions of the partial-wave expansion coefficients for general Bessel beams, given by Eqs. (7) and (10). Based on these analytical expressions, their partial derivatives with respect to x and y can be easily obtained:

$$\begin{aligned}
p^{(b)}_{mn,x} &= \frac{\partial p^{(b)}_{mn}}{\partial x} = -a\, i^{-m}\, e^{i(l-m)\phi_0} \\
&\quad\times \left[J'_{l-m}(a\rho_0)\cos\phi_0 - \frac{i(l-m)}{a\rho_0} J_{l-m}(a\rho_0)\sin\phi_0 \right] \\
&\quad\times \tilde{\pi}_{mn}(\cos\alpha), \\
p^{(b)}_{mn,y} &= \frac{\partial p^{(b)}_{mn}}{\partial y} = -a\, i^{-m}\, e^{i(l-m)\phi_0} \\
&\quad\times \left[J'_{l-m}(a\rho_0)\sin\phi_0 + \frac{i(l-m)}{a\rho_0} J_{l-m}(a\rho_0)\cos\phi_0 \right] \\
&\quad\times \tilde{\pi}_{mn}(\cos\alpha), \\
q^{(b)}_{mn,x} &= \frac{\partial q^{(b)}_{mn}}{\partial x} = -a\, i^{-m}\, e^{i(l-m)\phi_0} \\
&\quad\times \left[J'_{l-m}(a\rho_0)\cos\phi_0 - \frac{i(l-m)}{a\rho_0} J_{l-m}(a\rho_0)\sin\phi_0 \right] \\
&\quad\times \tilde{\tau}_{mn}(\cos\alpha), \\
q^{(b)}_{mn,y} &= \frac{\partial q^{(b)}_{mn}}{\partial y} = -a\, i^{-m}\, e^{i(l-m)\phi_0} \\
&\quad\times \left[J'_{l-m}(a\rho_0)\sin\phi_0 + \frac{i(l-m)}{a\rho_0} J_{l-m}(a\rho_0)\cos\phi_0 \right] \\
&\quad\times \tilde{\tau}_{mn}(\cos\alpha).
\end{aligned} \tag{20}$$

where the z_0 dependence e^{ibz_0} has been omitted. Then the analytical expressions for the FCM follow straightforwardly from Eqs. (13)–(17), considerably simplifying the linear stability analysis in the next section.

III. RESULTS AND DISCUSSION

With the formulations given in the previous section, we are ready to evaluate the optical force and FCM for a particle located arbitrarily in a Bessel beam. Recently, Siler *et al.* [59] discussed the behavior of a Rayleigh particle in a high-order Bessel beam. And the motion of the particle in the transverse plane was studied in their work. Here we study the behavior of a particle of arbitrary size in both zero- and high-order Bessel beams. The trajectories in both the transverse plane and the longitudinal direction are shown.

A. Bessel beams carrying AM

We focus on the case where the particle is near the transverse equilibrium at the beam axis. Due to the cylindrical symmetry of Bessel beams, one has $k_{11} = k_{22}$ and $k_{12} = -k_{21}$. The eigenvalues of the FCM reduce to

$$\lambda_\pm = k_{11} \pm i k_{12}. \tag{21}$$

Rewritten in radial and azimuthal components, the transverse optical force near the beam axis becomes

$$\boldsymbol{f}_t = \boldsymbol{e}_\rho\, f_\rho + \boldsymbol{e}_\phi\, f_\phi = \boldsymbol{e}_\rho\, k_{11} d + \boldsymbol{e}_\phi\, k_{12} d \quad \text{for} \quad kd \ll 1, \tag{22}$$

where $d = |\Delta \boldsymbol{x}|$ is the displacement of the particle from the beam axis, and $\boldsymbol{e}_\rho$ and $\boldsymbol{e}_\phi$ denote the unit vectors in the radial and azimuthal directions, respectively.

The transverse force given in Eq. (22) provides a transparent method for stability analysis. If $k_{11} > 0$, the particle will be driven away from the beam axis by the radial optical force $f_\rho > 0$ upon any perturbation. This transverse equilibrium is unstable and the NLOF near the beam axis in this case is therefore useless. When $k_{11} < 0$ and $k_{12} \neq 0$, the radial force plays the role of restoring the force, dragging the particle back to the beam axis when it drifts away. Nonvanishing azimuthal force, however, induces and accelerates particle rotation around the beam axis. If the ambient damping is not large enough to dissipate the rotation energy, the particle will deviate away from the beam axis due to the accumulation of AM acquiring from the beam, adding considerably to the complexity of optical pulling and largely limiting the applications. The critical damping constant for realizing transverse trapping is given by Refs. [28,36] $\gamma_{\text{critical}} = \sqrt{m_p}|\text{Im}(\lambda_\pm)|/\sqrt{|\text{Re}(\lambda_\pm)|}$, where m_p is the mass of the particle, which means that for $\gamma > \gamma_{\text{critical}}$ the particle can be bound to the beam axis. The favorable case corresponds to $k_{11} < 0$ and $k_{12} = 0$, where only negative radial optical force exists, and the particle will be bound to the beam axis irrespective of the ambient damping.

The nonzero azimuthal optical force, which makes the transverse equilibrium quasistable, is an inevitable result of the existence of rotating energy flux [28,36]. For optical vortex beams carrying AM, the resulting rotating energy flux will exert a torque on the particle and result in a nonzero k_{12}. Furthermore, the polarization state of the beam can also influence the value of k_{12} and we find that only a zero-order TE or TM polarized beam can induce zero azimuthal optical force. For Bessel beams, the rotating energy flux is independent of ϕ, reading

$$\begin{aligned}
\langle S_\phi \rangle &= \frac{1}{2}\text{Re}(\mathbf{E}\times\mathbf{H}^*)_\phi = \frac{1}{2} J_l^{\,2}(a\rho) \\
&\quad\times \left[\frac{la^2}{k\rho}(|c_1|^2 + |c_2|^2) - \frac{2a^3 b}{k^2}\,\text{Im}\,(c_1 c_2^*) D_l^{(1)}(a\rho) \right],
\end{aligned} \tag{23}$$

where $D_l^{(1)}(a\rho)$ is the logarithmic derivative of the Bessel function, given by $J'_l(a\rho)/J_l(a\rho)$. In some cases, as in Fig. 1(b) with $l = 0$, $c_1 = c_2 = 1$, although the rotating energy flux vanishes, the azimuthal optical force still exists.

If we expand the time-averaged optical force up to dipole order, we can obtain [4]

$$\mathbf{F} = \mathbf{F}_p + \mathbf{F}_m + \mathbf{F}_{pm} \ldots, \tag{24}$$

where

$$\begin{aligned}
\mathbf{F}_p &= \tfrac{1}{2}\text{Re}\{(\nabla \mathbf{E}^*)\cdot\mathbf{p}\}, \quad \mathbf{F}_m = \tfrac{1}{2}\text{Re}\{(\nabla \mathbf{B}^*)\cdot\mathbf{m}\}, \\
\mathbf{F}_{pm} &= -\frac{k^4}{12\pi\varepsilon_0 c}\text{Re}\{\mathbf{p}\times\mathbf{m}^*\}.
\end{aligned} \tag{25}$$

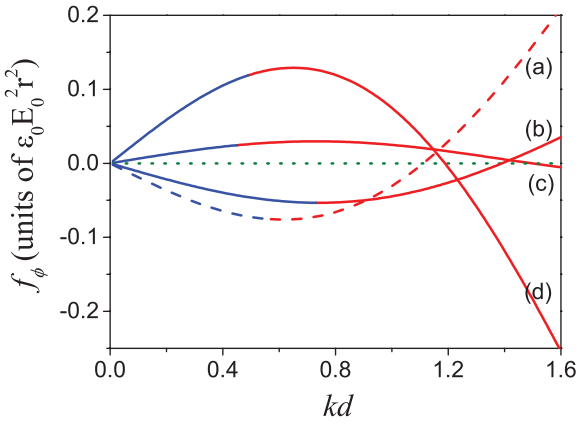

FIG. 1. (Color online) Azimuthal force f_ϕ versus displacement kd of the particle from the beam axis when it is illuminated by a Bessel beam with (a) $l = 1,\ c_1 = 1,\ c_2 = 0,\ \varepsilon = 6,\ kr = 2.6$; (b) $l = 0,\ c_1 = 1,\ c_2 = 1,\ \varepsilon = 2,\ kr = 3$; (c) $l = 0,\ c_1 = 1,\ c_2 = i,\ \varepsilon = 1.8,\ kr = 3$; and (d) $l = 1,\ c_1 = 1,\ c_2 = i,\ \varepsilon = 3.5,\ kr = 1.8$. The cone angle α of the incident Bessel beam is $\alpha = 70^\circ$ and the particle has permeability $\mu = 1$. Also shown, by color, is the longitudinal force f_z on the particle, with the (blue) color on the leftward portion of the curves denoting NLOF ($f_z < 0$) and that (red) on the rightward portion denoting PLOF ($f_z > 0$). Solid lines represent the radial optical force $f_\rho < 0$, corresponding to quasistable equilibrium due to $f_\phi \neq 0$, while dashed lines indicate $f_\rho > 0$, corresponding to unstable equilibrium at the beam axis.

The dipole moments are related to the incident field,

$$\mathbf{p} = \alpha_e \mathbf{E}, \quad \mathbf{m} = \alpha_m \mathbf{B}, \tag{26}$$

where $\alpha_e = i6\pi\varepsilon_0 a_1/k^3$ and $\alpha_m = i6\pi b_1/(k^3\mu_0)$, with (a_1, b_1) the Mie coefficients. Then the ϕ component of the optical force can be calculated as

$$(F_p)_\phi = \frac{3\pi\varepsilon_0}{k^3}\frac{l}{r}|\mathbf{E}|^2 \mathrm{Re}\{a_1\}, \tag{27a}$$

$$(F_m)_\phi = \frac{3\pi}{k^3\mu_0}\frac{l}{r}|\mathbf{B}|^2 \mathrm{Re}\{b_1\}, \tag{27b}$$

$$(F_{pm})_\phi = -\frac{3\pi}{k^2 c}\mathrm{Re}\{a_1 b_1^* \tilde{S}_\phi\}, \tag{27c}$$

where

$$\tilde{S}_\phi = (\mathbf{E}\times\mathbf{H}^*)_\phi = \frac{la^2}{k\rho}(|c_1|^2 + |c_2|^2)J_l^2 - \frac{2ia^3 b}{k^2}c_1^* c_2 J_l' J_l.$$

It therefore follows that for higher order Bessel beams (with $l > 0$), the azimuthal optical force does exist. As a result, a higher order Bessel beam cannot act as a tractor beam *per se* without the presence of ambient dissipation. Similarly, a nonzero k_{12} can also result from the polarization state of the beam. Since the Mie coefficients are complex numbers, the azimuthal optical force vanishes only when both the beam order l and $|c_1 c_2^*|$ are 0, namely, $l = 0$ plus $c_1 = 0$ or $c_2 = 0$ as indicated in Eq. (23). So to work in an arbitrary ambience, a favorable tractor beam *per se* is a zero-order Bessel beam with pure TM or TE polarizations.

First, we demonstrate some typical cases where NLOF is achieved near the beam axis, but with a nonzero azimuthal force f_ϕ that results from OAM for a beam with $l > 0$ or aspin AM (SAM) for a beam with $l = 0$ but $|c_1 c_2^*| \neq 0$. The results are shown in Fig. 1, where the azimuthal force f_ϕ is plotted as a function of the displacement kd of the particle from the beam axis and normalized by $\varepsilon_0 E_0^2 r^2$, with ε_0 the vacuum permittivity, E_0 the amplitude of the incident beam, and r the particle radius. The blue curves indicate that NLOF is exerted on the particle, while the red curves correspond to the cases when positive longitudinal optical force (PLOF) occurs. Therefore, we can find that when a particle is placed near the beam axis it is subject to NLOF; as it deviates from the beam axis, PLOF finally appears. Solid lines correspond to negative radial forces, $f_\rho < 0$, while dashed lines suggest positive radial force, $f_\rho > 0$. Accordingly, the case shown in curve a (Fig. 1) corresponds to an unstable equilibrium since the positive radial force $f_\rho > 0$ will drive the particle away from the beam axis. As a result, the NLOF near the beam axis (shown in blue) in this case does not allow for any practical application. For cases b to d, the radial force is negative (denoted by solid lines), playing the role of restoring force. One may naively believe that this corresponds to stable transverse confinement of the particle within the NLOF regime (shown in blue). This, however, is not the case, since the nonvanishing azimuthal force f_ϕ will stimulate a rotation of the particle around the beam axis once it deviates from the equilibrium at the beam axis. In a dissipationless environment, the rotation of the particle will be constantly accelerated, until it eventually moves to the PLOF regime (shown in red). This also prevents the application of NLOF near the beam axis, despite the presence of the restoring force $f_\rho < 0$. In some cases, the azimuthal optical forces may change sign as the displacement kd from the beam axis increases, as shown by curves b and d in Fig. 1. One may expect that the rotation of the particle around the beam axis may be first accelerated and then decelerated, leading to a complex trajectory near $f_\phi = 0$ but still confined within the region of NLOF. However, our numerical results show that this is not the case either, because the longitudinal forces always become positive before the azimuthal force change its sign. This is typically shown in Fig. 1 by curves b and d, where the curves change from blue to red, indicating that the particle enters the PLOF regime before f_ϕ changes its sign. So the particle may at best be stabilized transversely in the region with PLOF, spoiling the phenomenon of optical pulling.

To gain further insight into the stability of NLOF, a dynamical simulation of the particle trajectory is necessary and, also, sufficient to provide a clear picture of the evolution of the particle in Bessel beams. The dynamic simulations integrate the equation of motion, $m_p d^2\Delta\boldsymbol{x}/dt^2 = \boldsymbol{f}_{\text{light}} - \gamma d\Delta\boldsymbol{x}/dt$, using an adaptive time step Runge-Kutta-Verner algorithm [36]. In Fig. 2, we present corresponding results where the motion of the particle in both the transverse plane and along the longitudinal direction is simulated. For the cases shown in Figs. 2(a)–2(d), the particle is illuminated by a Bessel beam with $l = 0,\ c_1 = 1,\ c_2 = 1$, indicating a beam with SAM and without OAM, corresponding to the curve in Fig. 1(b). As shown in Fig. 2(a), the particle is driven far away from its initial location near the beam axis in a dissipationless environment. As a result, the particle is pulled backward to the source due to NLOF when it is close to the beam axis in the early stage and then it drifts into the region of PLOF and is finally pushed away from the light source when the particle deviates away from the beam axis, whichis clearly illustrated in Fig. 2(b). This is in

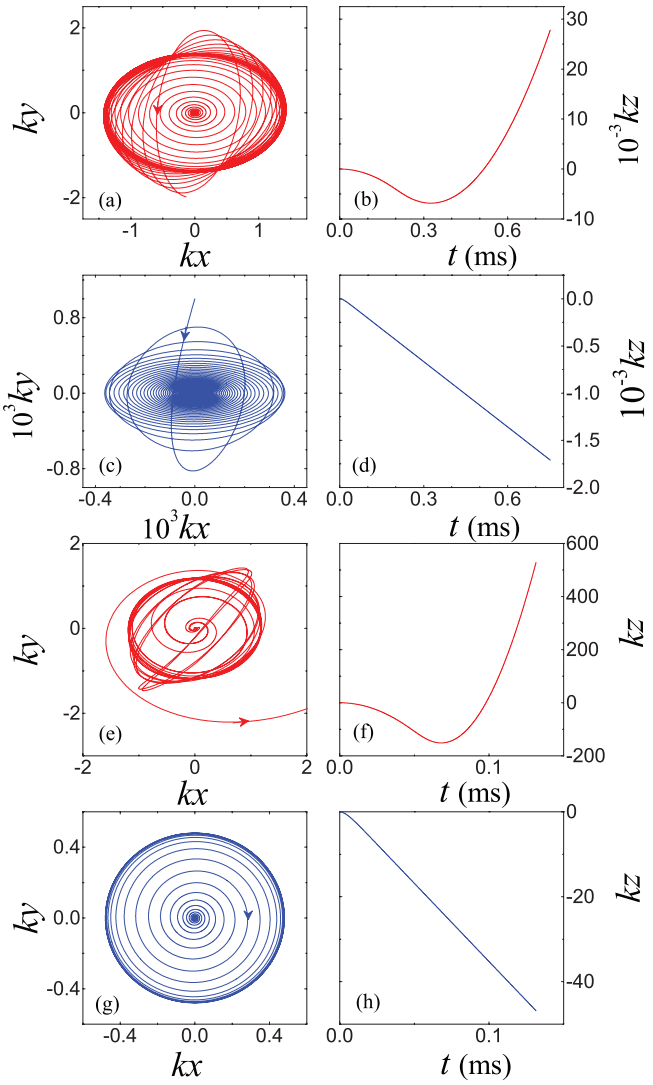

FIG. 2. (Color online) Dynamical simulation of the trajectories for a dielectric particle with $kr = 3$ and $\varepsilon = 2$ (a)–(d) and $kr = 1.8$ and $\varepsilon = 3.5$ (e)–(h) in the transverse plane (a), (c), (e), (g) and in the z direction (b), (d), (f), (h), when it is illuminated by a Bessel beam with $l = 0$, $c_1 = 1$, $c_2 = 1$ (a)–(d) and $l = 1$, $c_1 = 1$, $c_2 = i$ (e)–(h), corresponding to curves b and d in Fig. 1, respectively. In the dynamical simulations, (a), (b), (e), and (f) correspond to cases without ambient damping; (c) and (d), cases with the damping constant $\gamma/\gamma_{\text{critical}} = 1.2$; and (g) and (h), cases with the damping constant $\gamma/\gamma_{\text{critical}} = 0.8$. The cone angle of the Bessel beam is $\alpha = 70^\circ$ and the particle is initially located at $kd = 0.001$ with zero velocity. Arrows indicate the directions of the motion. The density of the particles is $\rho_p = 1050\ \text{kg/m}^3$, the wavelength is $\lambda = 1\ \mu\text{m}$, and $E_0 = 1\ \text{V/m}$.

agreement with curve b in Fig. 1 in that the azimuthal force f_ϕ due to SAM leads to quasistable NLOF. But the situation may change in the presence of damping, as illustrated in Figs. 2(c) and 2(d) with damping constant $\gamma/\gamma_{\text{critical}} = 1.2$, where the ambient damping dissipates the rotation energy that the particle acquires from the beam carrying SAM. Therefore, the particle is attracted back to the beam axis after a complicated orbiting trajectory in the transverse plane and then fixed there so that a stable NLOF can be obtained. In Figs. 2(e)–2(h), we also present the dynamical simulation of the same particle illuminated with a Bessel beam with $l = 1$, $c_1 = 1$, $c_2 = i$, corresponding to curve d in Fig. 1, so that both OAM and SAM are delivered to the particle. It is shown that in the absence of ambient damping, the particle initially located very close to the beam axis will eventually run away, as displayed in Fig. 2(e). As the particle deviates away from the beam axis, it enters the region of PLOF and, finally, is pushed away from the light source, as shown in Fig. 2(f). However, when the damping constant $\gamma/\gamma_{\text{critical}} = 0.8$ is considered, although the particle deviates from the beam axis, after a complicate trajectory it is confined in the NLOF region as shown in Fig. 2(g), resulting in a stable NLOF. Accordingly, as in the case in Fig. 2(d), it also moves longitudinally in the direction opposite to the beam propagation due to the optical pulling force, rendering NLOF applicable for long-distance backward particle transportation. This may be termed "optohydrodynamic" optical pulling, namely, the optical pulling is stabilized by ambient damping, analogous to optohydrodynamic trapping by an optical beam carrying AM [28].

The need for ambient damping, which depends on the particle itself as well as the surrounding medium, adds considerably to the difficulty of analysis on optical pulling using beams carrying AM, either OAM or SAM. We leave this discussion to a separate publication. In the following, we focus our study on Bessel beams carrying no AM.

B. Bessel beams carrying no AM

In this section, we focus on the stability analysis of a particle illuminated by zero-order Bessel beams of pure TM ($c_1 = 0$) or TE ($c_2 = 0$) polarization, so that the Bessel beams do not induce any azimuthal optical force. The advantages of using such Bessel beams are obvious: (i) the environment is no longer the critical aspect for obtaining stable NLOF since the restoring force itself is capable of realizing transverse equilibrium, simplifying the analysis; and (ii) due to the absence of azimuthal optical force, the trajectory of the particle will be much simpler, which makes it easily visualized in the dynamical simulation.

The phase diagram is a powerful means to acquire knowledge of NLOF, thus in Fig. 3, we present the phase diagrams

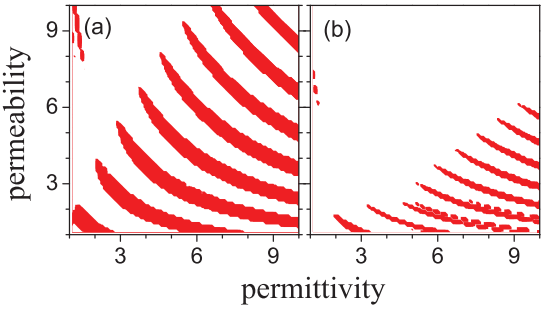

FIG. 3. (Color online) Phase diagrams of NLOF with respect to the permittivity and the permeability of a particle located on the beam axis of a zero-order incident Bessel beam with $\alpha = 70^\circ$, $c_1 = 1$, and $c_2 = 0$ (TE beam). The size of the particle is $kr = 3$ (a) and $kr = 4.5$ (b), respectively. White and dark (red) regions denote PLOF and NLOF, respectively.

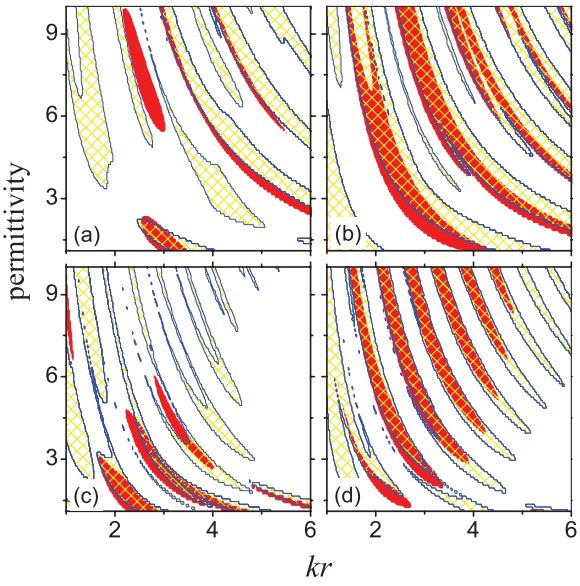

FIG. 4. (Color online) Phase diagrams with respect to the particle size kr and the permittivity, which illustrate NLOF [dark (red) regions], PLOF (white regions), and unstable phase [light (yellow) regions] for a particle under the illumination of a zero-order incident Bessel beam with $\alpha = 70^\circ$ when it is placed on the beam axis. Other parameters are (a) $c_1 = 0$, $c_2 = 1$, $\mu = 1$; (b) $c_1 = 1$, $c_2 = 0$, $\mu = 1$; (c) $c_1 = 0$, $c_2 = 1$, $\mu = 1.5$; and (d) $c_1 = 1$, $c_2 = 0$, $\mu = 1.5$.

with respect to the permittivity and the permeability of a particle when it is illuminated by a zero-order Bessel beam of pure TE polarization. As shown in Fig. 3(a), dark (red) areas indicate the parameter space where NLOF occurs when the particle is placed on the beam axis. White regions correspond to the parameter space where PLOF appears. We can also find that NLOF exists mostly in regions of $\varepsilon > \mu$, indicating that a TE beam is more favorable for achieving NLOF than a TM beam for a conventional nonmagnetic dielectric particle with $\mu = 1$. In addition, particle size also has an obvious influence on NLOF, as shown in the phase diagram in Fig. 3(b), where a larger particle with $kr = 4.5$ is considered. Compared to that in Fig. 3(a), the NLOF region shrinks considerably for large particles.

Based on the phase diagram, we can also obtain information on the stability of NLOF as well as the polarization dependence. For this purpose, we present in Fig. 4 the phase diagrams of NLOF with respect to the particle size and permittivity, where dark (red) regions denote the parameter spaces for the occurrence of NLOF, while white regions correspond to PLOF when the particle is under the on-axis illumination of either TM [Figs. 3(a) and 3(c)] or TE [Figs. 3(b) and 3(d)] beams. The stability of the phase is also illustrated in Fig. 4, where the light (yellow) regions indicate parameter spaces corresponding to positive eigenvalues for the FCM, suggesting unstable on-axis equilibrium. Unshaded regions correspond to the stable phase; that is, the particle can be confined around the beam axis due to the negative radial force $f_\rho < 0$ in the transverse plane. Accordingly, the dark (solid red) regions represent parameter spaces for stable NLOF, so that long-distance optical pulling is achievable. Since magnetic moments play an important role for NLOF [4], the NLOF phase induced by a TM polarized beam

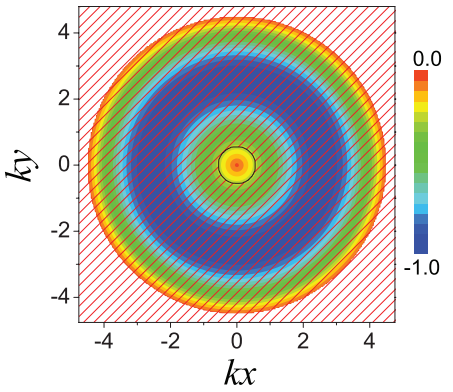

FIG. 5. (Color online) The radial optical force f_ρ (arbitrary units) is plotted as a function of the particle position in the transverse plane when it is illuminated by a zero-order TM Bessel beam with $\alpha = 70^\circ$. The particle has permittivity $\varepsilon = 7$, permeability $\mu = 1$, and particle size $kr = 2.7$. Colored areas denote $f_\rho < 0$, and white areas denote $f_\rho > 0$. Regions hatched with (red) lines represent locations for realization of PLOF, while unhatched regions in central areas denote locations for realization of NLOF.

for nonmagnetic particles is much weaker and more sensitive to the particle permittivity as shown in Fig. 4(a). But for magnetic particles, NLOF induced by a TM polarized beam will be strengthened, and the permittivity for NLOF will decrease as shown in Fig. 4(c). In contrast, for a TE polarized beam, a magnetic response ($\mu = 1.5$) has a relatively weaker influence on NLOF by comparing Figs. 4(b) and 4(d). Although the instability in transverse equilibrium, which occurs even for the PLOF phase, prevents much of the NLOF phase from being used in practical applications for optical pulling, it suggests another application for optical sorting and selection [33,60,61]. In addition, from the phase diagrams in Fig. 4 we also find different tendencies of permittivity for the stable transverse equilibrium. For the TE polarized beam, stable NLOF is likely achieved when the particle permittivity is small, while for the TM polarized beam, a particle with wide ranges of large permittivity can be captured. This property guides us to choose suitable Bessel beams for particle operations.

However, in practical situations, a particle is usually located at an off-axis position. The stability of NLOF in this case should be appropriately analyzed. To this end, we calculate the radial optical force f_ρ acting on a particle as a function of the particle position in the transverse plane. A typical result is shown in Fig. 5 for a nonmagnetic particle under the illumination of a zero-order TM Bessel beam. The negative radial force, $f_\rho < 0$, is shown in color, while white regions display the areas for $f_\rho > 0$. In regions hatched with solid (red) lines, the particle is subject to PLOF, $f_z > 0$, and in unhatched regions, which appear around the beam axis, the particle is subject to NLOF. In the outer hatched white regions, the particle is subject to PLOF and positive radial force simultaneously. Thus, it will be driven away from the beam axis and, finally, escape. However, for a particle placed in the middle hatched color regions, the situation is a little bit complicated. The negative radial force tends to drag the particle back to the beam axis, resulting in a transition of the longitudinal force from PLOF in the hatched regions to

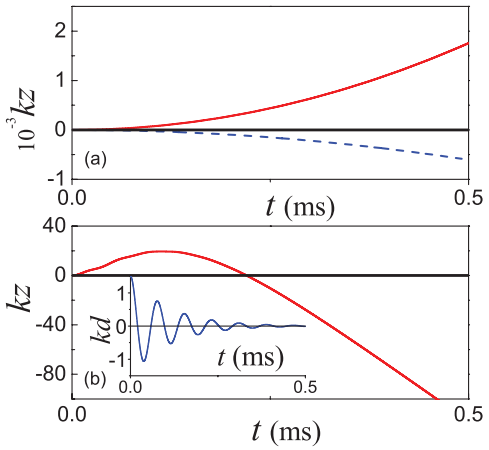

FIG. 6. (Color online) Trajectories of a nonmagnetic particle with $kr = 2.7$ and $\varepsilon = 7$ under illumination of a zero-order TM Bessel beam. Longitudinal components along the z direction for an environment without damping (a) and with damping (b). (a) The dashed (blue) line and solid (red) line correspond to particle trajectories with initial positions at $kd = 0.5$ and $kd = 1.5$, respectively. (b) The solid (blue) line in the inset denotes the corresponding trajectory in the transverse plane. The density of the particle is $\rho_p = 1050$ kg/m^3, $\lambda = 1$ μm, $E_0 = 1$ V/m.

NLOF in the regions around the beam axis shown in Fig. 5 by the inner unhatched color region. Then, due to the inertia of the particle, it will move away from the beam center and a transition from NLOF to PLOF occurs. Therefore, in the transverse plane the particle will oscillate around the beam axis and it will locate alternatively in NLOF and PLOF regions.

Dynamical simulations can provide further insight into the phenomenon by observing the particle motion. In Fig. 6, we present the trajectory of a particle in an undamping and a damping environment in Figs. 6(a) and 6(b), respectively. The dashed (blue) line and the solid (red) line correspond to the longitudinal trajectories for a dielectric particle with initial positions at $kd = 0.5$ and $kd = 1.5$, respectively. As shown in Fig. 5, the initial longitudinal optical force is NLOF and PLOF, respectively, for the two cases, resulting in stable longitudinal motion along the negative and positive directions. It is noted that although the negative radial force can drag the particle to the NLOF region, the particle keeps moving along the positive direction as shown by the solid (red) line in Fig. 6(a). Differently, in the damping environment the oscillation of the particle is weakened quickly so that it is finally confined in the NLOF region as shown by the solid (blue) line in the inset in Fig. 6(b). Accordingly, the particle first experiences a motion along the positive direction and then moves backward to the source along the negative direction as indicated by the solid (red) line in Fig. 6(b). Ambient damping can induce stable NLOF once again as in the case discussed for Fig. 2 for a beam with AM by dissipating the undesirable energy. At any rate, stable NLOF *per se* in the absence of ambient damping occurs only in the unhatched color region around the beam center in Fig. 5 due to the confinement of the particle by the negative radial optical force $f_\rho < 0$.

For convenience, we define the radius of the unhatched color region in Fig. 5 as r_c. Inside this region, stable NLOF can be realized in the absence of ambient damping. To determine what particle can be stably pulled back by a specified Bessel beam with a required r_c, we present the phase diagrams in Fig. 7, where the colored stripes are the same as those shown in Figs. 4(a) and 4(b), given here for comparison, while the unhatched darker (red) regions in Figs. 7(a) and 7(b) show, respectively, the stable off-axis NLOF phase for a TM beam with $kr_c = 0.4$ and a TE beam with $kr_c = 0.8$. The phase diagram suggests a possible application, namely, if one shines a zero-order Bessel beam on an aggregate of particles made of different materials, then a particle with parameters in the dark (red) region of the phase diagram will be stably confined in the NLOF region when its distance d from the beam center satisfies $kd < kr_c$. For particles with the parameters in the hatched region, however, the Bessel beam exerts NLOF on the particle when it is on the beam axis, but optical pulling may not work due to transverse instability.

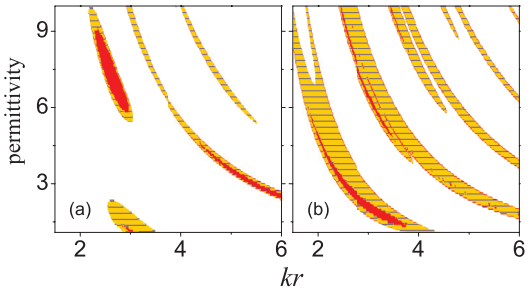

FIG. 7. (Color online) Phase diagrams with respect to the particle size kr and the permittivity for a nomagnetic particle under the illumination of zero-order TM (a) and TE (b) Bessel beams with $\alpha = 70°$. Colored areas show the parameter spaces in which the NLOF phase occurs when the particle is placed on the beam axis, which are the same as those shown in Figs. 4(a) and 4(b), respectively. Solid (red) regions denote the stable NLOF phase when the particle deviates from the beam axis at $kr_c = 0.4$ and $kr_c = 0.8$; striped (yellow) regions denote the unstable NLOF phase.

IV. SUMMARY

To summarize, based on the generalized Lorenz-Mie theory and the Maxwell stress tensor formulism, we have derived analytical expressions for the optical force and FCM for a particle illuminated by a Bessel beam of arbitrary order and polarization. By calculating the phase diagrams, we can discriminate the NLOF phase from the PLOF phase within a specified parameter space associated with the particle. In addition, by considering the radial optical force in the transverse plane we can also search out the stable NLOF phase for a particle placed on or off the beam axis. Dynamical simulations have been performed as well to depict the trajectories of a particle from its initial position under the illumination of a Bessel beam. Our numerical results show that a particle cannot be stably confined in the NLOF region by higher order Bessel beams in the absence of ambient damping. The physics lies in the fact that AM carried by the higher order Bessel beam will stimulate and accelerate the rotation of the particle around the beam axis, and eventually drive the particle away. As ambient damping plays an important role in the realization of stable NLOF for higher order Bessel beams,

the phenomenon of optical pulling based on higher order Bessel beams may be termed "optohydrodynamic pulling," analogous to "optohydrodynamics trapping" using an optical vortex [36], to identify its non-purely-optical characteristics like thermal photophoretic forces [62]. A zero-order Bessel beam with pure TM or TE polarization can implement stable transverse confinement, acting as an optical tractor beam *per se*, irrespective of the ambience. This corresponds to the stable NLOF phase in the phase diagrams. In addition, for a nonmagnetic particle, a TE Bessel beam is more suitable for realizing NLOF than a TM beam. Finally, a brief discussion has also been presented on the backward transportation of a particle located either on or off the beam axis using NLOF.

ACKNOWLEDGMENTS

The work was supported by the National Natural Science Foundation of China (Grants No. 11174059 and No. 11274277), the MOE of China (Grant No. B06011), and the open project SKLSP at Fudan University (No. KL2011_8).

[1] S. H. Lee, Y. Roichman, and D. G. Grier, Opt. Express **18**, 6988 (2010).
[2] S. Sukhov and A. Dogariu, Opt. Lett. **35**, 3847 (2010).
[3] S. Sukhov and A. Dogariu, Phys. Rev. Lett. **107**, 203602 (2011).
[4] J. Chen, J. Ng, Z. F. Lin, and C. T. Chan, Nature Photon. **5**, 531 (2011).
[5] J. Saenz, Nature Photon. **5**, 574 (2011).
[6] A. Novitsky, C. W. Qiu, and H. Wang, Phys. Rev. Lett. **107**, 203601 (2011).
[7] A. Novitsky, C. W. Qiu, and A. Lavrinenko, Phys. Rev. Lett. **109**, 023902 (2012).
[8] D. B. Ruffner and D. G. Grier, Phys. Rev. Lett. **109**, 163903 (2012).
[9] T. Kudo and H. Ishihara, Phys. Rev. Lett. **109**, 087402 (2012).
[10] A. Dogariu, S. Sukhov, and J. J. Saenz, Nature Photon. **7**, 24 (2013).
[11] O. Brzobohaty, V. Karasek, M. Siler, L. Chvatal, T. Cizmar, and P. Zemanek, Nature Photon. **7**, 123 (2013).
[12] P. L. Marston, J. Acoust. Soc. Am. **120**, 3518 (2006); **122**, 3162 (2007); **125**, 3539 (2009).
[13] F. G. Mitri, J. Phys. A: Math. Theor. **42**, 245202 (2009).
[14] L. Zhang and P. L. Marston, Phys. Rev. E **84**, 035601 (2011); J. Acoust. Soc. Am. **131**, EL329 (2012).
[15] S. J. Xu, C. Y. Qiu, and Z. Y. Liu, Europhys. Lett. **99**, 44003 (2012).
[16] A. Ashkin, Phys. Rev. Lett. **24**, 156 (1970); A. Ashkin, J. M. Dziedzic, J. E. Bjorkholm, and S. Chu, Opt. Lett. **11**, 288 (1986).
[17] D. G. Grier, Nature (London) **424**, 810 (2003).
[18] K. C. Neuman and S. M. Block, Rev. Sci. Instrum. **75**, 2787 (2004).
[19] K. Dholakia and P. Reece, Nano Today **1**, 18 (2006).
[20] A. Ashkin, *Optical Trapping and Manipulation of Neutral Particles Using Lasers: A Reprint Volume with Commentaries* (World Scientific, Singapore, 2006).
[21] J. Baumgartl, M. Mazilu, and K. Dholakia, Nature Photon. **2**, 675 (2008).
[22] G. A. Swartzlander Jr., T. T. Peterson, A. B. Artusio-Glimpse, and A. D. Raisanen, Nature Photon. **5**, 48 (2011).
[23] K. Dholakia1 and T. Čižmár, Nature Photon. **5**, 335 (2011).
[24] M. Padgett and R. Bowman, Nature Photon. **5**, 343 (2011).
[25] L. Allen, M. W. Beijersbergen, R. J. C. Spreeuw, and J. P. Woerdman, Phys. Rev. A **45**, 8185 (1992).
[26] A. M. Yao and M. J. Padgett, Adv. Opt. Photon. **3**, 161 (2011).
[27] S. H. Simpson and S. Hanna, J. Opt. Soc. Am. A **27**, 2061 (2010).
[28] J. Ng, Z. F. Lin, and C. T. Chan, Phys. Rev. Lett. **104**, 103601 (2010).
[29] J. Durnin, J. Opt. Soc. Am. A **4**, 651 (1987); J. Durnin, J. J. Miceli, and J. H. Eberly, Phys. Rev. Lett. **58**, 1499 (1987).
[30] Z. Bouchal and M. Olivik, J. Mod. Opt. **42**, 1555 (1995).
[31] J. Arlt, V. Garces-Chavez, W. Sibbett, and K. Dholakia, Opt. Commun. **197**, 239 (2001).
[32] J. Tervo, P. Vahimaa, and J. Turunen, J. Mod. Opt. **49**, 1537 (2002).
[33] D. McGloin and K. Dholakia, Contemp. Phys. **46**, 15 (2005).
[34] J. Turunen and A. T. Friberg, in *Progress in Optics*, Vol. 54 (Elsevier, Amsterdam, 2009), Chap. 1.
[35] M. Mazilu, D. J. Stevenson, F. Gunn-Moore, and K. Dholakia, Laser Photon. Rev. **4**, 529 (2010).
[36] J. Ng, Z. F. Lin, C. T. Chan, and P. Sheng, Phys. Rev. B **72**, 085130 (2005).
[37] K. Dholakia and P. Zemanek, Rev. Mod. Phys. **82**, 1767 (2010).
[38] G. Gouesbet, J. Quant. Spectrosc. Radiat. Transf. **110**, 1223 (2009).
[39] G. Gouesbet and G. Grehan, *Generalized Lorenz-Mie Theories* (Springer, Berlin, 2011).
[40] G. Gouesbet and J. A. Lock, Appl. Opt. **52**, 897 (2013).
[41] J. A. Stratton, *Electromagnetic Theory* (McGraw–Hill, New York, 1941).
[42] C. F. Bohren and D. R. Huffman, *Absorption and Scattering of Light by Small Particles* (John Wiley and Sons, New York, 1983).
[43] Z. F. Lin and S. T. Chui, Phys. Rev. E **69**, 056614 (2004).
[44] J. Chen, J. Ng, S. Y. Liu, and Z. F. Lin, Phys. Rev. E **80**, 026607 (2009).
[45] J. Chen, J. Ng, P. Wang, and Z. F. Lin, Opt. Lett. **35**, 1674 (2010); **36**, 1243(E) (2011).
[46] G. Gouesbet, Opt. Commun. **283**, 517 (2010).
[47] L. Mandel and E. Wolf, *Optical Coherence and Quantum Optics* (Cambridge University Press, Cambridge, 1995).
[48] L. Novotny and B. Hecht, *Principles of Nano-Optics* (Cambridge University Press, Cambridge, 2006).
[49] K. F. Ren, G. Grehan, and G. Gouesbet, Opt. Commun. **108**, 343 (1994).
[50] K. F. Ren, G. Grehan, and G. Gouesbet, Appl. Opt. **35**, 2702 (1996).
[51] H. Polaert, G. Grehan, and G. Gouesbet, Appl. Opt. **37**, 2435 (1998).
[52] H. Polaert, G. Grehan, and G. Gouesbet, Opt. Commun. **155**, 169 (1998).

[53] J. D. Jackson, *Classical Electrodynamics*, 3rd ed. (Wiley, New York, 1999).
[54] J. P. Barton, D. R. Alexander, and S. A. Schaub, J. Appl. Phys. **66**, 4594 (1989).
[55] O. Farsund and B. U. Felderhof, Physica A **227**, 108 (1996).
[56] R. Pobre and C. Saloma, Appl. Opt. **41**, 7694 (2002).
[57] M. K. Liu, N. Ji, Z. F. Lin, and S. T. Chui, Phys. Rev. E **72**, 056610 (2005).
[58] A. Salandrino, S. Fardad, and D. N. Christodoulides, J. Opt. Soc. Am. B **29**, 855 (2012).
[59] M. Siler, P. Jakl, O. Brzobohaty, and P. Zemanek, Opt. Express **20**, 24304 (2012).
[60] M. P. MacDonald1, G. C. Spalding, and K. Dholakia, Nature **426**, 421 (2003).
[61] J. Ng and C. T. Chan, Appl. Phys. Lett. **92**, 251109 (2008).
[62] V. G. Shvedov, A. V. Rode, Y. V. Izdebskaya, A. S. Desyatnikov, W. Krolikowski, and Y. S. Kivshar, Phys. Rev. Lett. **105**, 118103 (2010).